International Journal of Materials Science

E-ISSN: 2707-823X
P-ISSN: 2707-8221
IJMS 2023; 4(2): 22-27
Received: 22-04-2023
Accepted: 26-05-2023

Hugo Jhonathan Marín García
Instituto de Investigación en Metalurgia y Materiales, Universidad Michoacana de San Nicolás de Hidalgo, Edif. "U", Av. Fco. J. Múgica S/N, Ciudad Universitaria, C.P. 58030 Morelia, Michoacán de Ocampo, México

Ramiro Escudero García
Instituto de Investigación en Metalurgia y Materiales, Universidad Michoacana de San Nicolás de Hidalgo, Edif. "U", Av. Fco. J. Múgica S/N, Ciudad Universitaria, C.P. 58030 Morelia, Michoacán de Ocampo, México

Ricardo Morales Estrella
Instituto de Investigación en Metalurgia y Materiales, Universidad Michoacana de San Nicolás de Hidalgo, Edif. "U", Av. Fco. J. Múgica S/N, Ciudad Universitaria, C.P. 58030 Morelia, Michoacán de Ocampo, México

Corresponding Author:
Ramiro Escudero García
Instituto de Investigación en Metalurgia y Materiales, Universidad Michoacana de San Nicolás de Hidalgo, Edif. "U", Av. Fco. J. Múgica S/N, Ciudad Universitaria, C.P. 58030 Morelia, Michoacán de Ocampo, México

Dissolution of vanadium and titanium from a titaniferous beach sand by the oxidation, carbothermal reduction and acid leaching route

Hugo Jhonathan Marín García, Ramiro Escudero García and Ricardo Morales Estrella

Abstract
Titanium and vanadium metals are used in the manufacture of micro alloyed steels, medical instruments, automobile parts, among others. The beaches of Mexico along the Pacific Ocean have sands called "titaniferous", rich in mineral species of iron, vanadium and titanium, mainly.
This work proposes the dissolution of Fe, Ti and V, contained in the beach sand, after its oxidation and carbothermal reduction, for the subsequent recovery of the metals; for example, by cementation.
The chemical characterization of the beach sand, by means of atomic absorption spectroscopy (EAA) and mass ICP (ICP-OES)), indicates that this mineral contains 65.85% (w/w) of Fe, in addition to 1.17 and 0.35% (w/w), titanium and vanadium, respectively. Analysis by X-ray diffraction (XRD) indicates the presence of the mineral phases: magnetite, iron-silicon oxide and iron-titanium oxide. Scanning electron microscopy (SEM) analysis shows a compact morphology with little irregularity. The mineral sample was pulverized to a D80 particle size of 86 µm for its subsequent treatment. The oxidation of the mineral was carried out with hot air, for the carbothermal reduction graphite was used as a reducing agent, so that in this way it was possible to dissolve Fe, Ti and V in an acid medium, for its subsequent recovery.
After oxidation in the mineral sand, the α-hematite phase was identified. The result of the reduction was the obtaining of elemental iron and titanium carbide (khamrabaevite). Finally, the reduced ore was leached with an acid solution (3% HCl for 48 h), completely dissolving iron and vanadium, while titanium dissolved 76.92% of its original content.

Keywords: Carbothermal reduction, titaniferous beach sand, oxidation, acid leaching, titanium, vanadium

Introduction
Extractive metallurgy and mining are related to obtaining metals from the corresponding minerals [1]. In the case of titanium and vanadium, both belong to the transition metal group of the periodic table, having their "d" subshells incomplete and easily give rise to ions that have these subshells incomplete, giving them several outstanding chemical properties, such as catalytic activity, marked tendency to form complex ions, among others [2]. For titanium there are two main mineral species, titanium dioxide (TiO_2), commonly in black or brown color known as rutile, the anatase, and broochite (these two forms being less frequent), and iron-titanium oxide ($FeTiO_3$), black in color called ilmenite, which is the main commercial source of this element [3]. As for vanadium, it is not found in an elemental form in nature, but it is found in a wide variety of minerals; in its pure metallic form, it is shiny gray, soft, and ductile [4].
The titaniferous mineral comes from black or alluvial sands, product of the accumulation of valuable mineral that is deposited with sediments in the bed of a water current or flood zone, such as river and sea beaches; this deposit generally consists of magnetite (Fe_3O_4), and ilmenite ($FeTiO_3$) associated with garnet, rutile and zircon [5]. Beach minerals have been subjected to concentrations to increase the percentage of iron oxides and reduce the content of silicate and non-magnetic minerals (feldspars, quartz, chlorite, amphiboles, pyroxene, among others) [6, 7]. Regarding the carbothermal reduction of oxides or oxidized minerals, the reducing agent is coal, where the product of this operation can be a metal (Tin or zinc), a cemented metal (iron) or a carbide (chromium, titanium, aluminum); In the case of ilmenite, it is carried out in rotary kilns at 1200 °C, for 8 to 9 h to obtain an almost total reduction of the iron oxide that constitutes the species, while the titanium is separated by leaching [8].

Once again, Vargas *et al.* [7] pelletized the ore with diluted molasses, later coke was added to one part, and they were directly subjected to electric arc fusion; the other part was oxidized (hematized) at 1150 °C for 4 h to facilitate its carbothermal reduction, since magnetite lacks permeability and is very dense, concluding that the best behavior in the furnace occurred in the oxidized mineral. Finally, Yang *et al.* [9] studied the isothermal mechanism of hematite reduction in pellets added with graphite, indicating two types of reactions: indirect (eq. 1 to 3), accompanied by the carbon gasification reaction (eq. 4), known as Boudouard reaction; and direct (eq. 5 to 7), together with the wustite reaction with dissolved carbon (eq. 8), and the carburization reaction (eq.9).

$$< 3Fe_2O_3 > +(CO) \leftrightarrow < 2Fe_3O_4 > +(CO_2) \quad \text{(eq. 1)}$$

$$< Fe_3O_4 > +(CO) \leftrightarrow < 3FeO > +(CO_2) \quad \text{(eq. 2)}$$

$$< FeO > +(CO) \leftrightarrow < Fe > +(CO_2) \quad \text{(eq. 3)}$$

$$< C > +(CO_2) \leftrightarrow (2CO) \quad \text{(eq. 4)}$$

$$< 3Fe_2O_3 > +< C > \leftrightarrow < 2Fe_3O_4 > +(CO) \quad \text{(eq. 5)}$$

$$< Fe_3O_4 > +< C > \leftrightarrow < 3FeO > +(CO) \quad \text{(eq. 6)}$$

$$< FeO > +< C > \leftrightarrow < Fe > +(CO) \quad \text{(eq. 7)}$$

$$< FeO > +[C] \leftrightarrow < Fe > +(CO) \quad \text{(eq. 8)}$$

$$< C > \leftrightarrow [C] \quad \text{(eq. 9)}$$

On the other hand, the carbothermal reduction process of mechanically activated ilmenite ($FeTiO_3$) was studied by Welham *et al.* [10], also analyzing the reduction of rutile (TiO_2) in order to remove the effect of iron in the late stages of reaction, identifying in the ilmenite diffractograms the presence of more graphite, than from 700 °C the reduction is clear with the appearance of the rutile and elemental iron peaks, while at 800 °C the reduction is complete. Regarding the behavior of rutile, intermediate phases of titanium oxides appear and by increasing the proportion of graphite, the formation of titanium carbide (TiC) is favored. Likewise, when leaching the ilmenite reduction products, 90% of the iron dissolved after 800 °C, and almost complete dissolution was reached after 1000 °C; Titanium and iron separation is maximized when TiC and Fe are present above 1200 °C.

Methodology

Ore preparation

The titaniferous sand was named as head mineral (MCab), it was homogenized to obtain a representative sample of approximately 100 kg; said sample was pulverized in a disc mill, in order to improve the release of species; the pulverized sample was quartered and around 1 kg of mineral sample was obtained. The particles were classified by size according to the Tyler No. 70, 100, 200 and 270 sieves (+214, +149, +74, +54 µm, respectively).

Chemical analysis of the oral

To carry out the chemical characterization of the mineral samples, the following analysis techniques were applied: X-ray fluorescence (XRF, Spectro Xepos AMETEK), X-ray diffraction (XRD, SIEMENS D5000), field emission scanning electron microscopy (SEM, JEOL JSM-7600F FEG-SEM, secondary and backscattered electron mode). To quantify titanium, vanadium iron and precious metals, the technique of optical emission spectroscopy coupled to plasma induction (ICP-OES) and flame atomic absorption spectroscopy (EAAF) was applied with previous microwave-assisted chemical digestion (Multiwave 3000 Anton Para) with HCl at 3%.

Carbothermal oxidation and reduction of the ore

The oxidation process began with the thermogravimetric analysis (TGA) of particles between 150 and 75 µm in size, in an air atmosphere; Subsequently, the mineral was subjected to 950 °C with residence times of 6, 12 and 24 hours, always with an air supply. Regarding the reduction process, the oxidized mineral and the graphite were mixed in a 1:4 molar ratio (MMez), the mixture was placed in a covered graphite crucible and this was subjected to 1100 °C with 4 h of permanence in an atmosphere of air in a horizontal tube furnace, for both stages the resulting mineral was analyzed by DRX and MEB.

Acidic leaching

The leaching of the head mineral, the oxidized mineral (MOxi), and the reduced mineral (MRed), was carried out in an open manner and with a diluted 3% HCl solution for 48 h, with a change of solution after 24 h. The obtained solutions were analyzed by ICP-OES and EAAF.

Results and Discussion

The results of the elemental analysis by XRF are shown in Table 1. It is observed that iron is the one with the highest proportion (65.84%, w/w), which presented magnetic behavior, followed by silicon, sodium, magnesium, and much lower, calcium, among others, which mostly make up the non-metallic minerals and are discarded in the previous magnetic concentration [7]. Among the metals of interest, four main elements were found, highlighting the presence of titanium and vanadium [7, 11]. However, due to the sensitivity of the technique, the presence of precious metals such as gold and silver was not detected.

Table 1: Chemical analysis (% w/w) by the X-ray Fluorescence technique of titaniferous beach sand.

Element	%, (w/w)	Element	%, (w/w)
Fe	65.85	Mn	0.21
Si	4.88	P	0.11
Na	3.23	K	0.11
Ti	2.79	Cr	0.09
Al	1.72	S	0.02
Mg	1.46	Cl	0.01
Ca	0.91	Others	<18.31
V	0.61		

The mineral phases indexed by XRD in the MCab were magnetite JCPDS-00-019-0629 (Fe_3O_4, cubic structure), iron-silicon oxide JCPDS-00-052-1140 ($Fe_{2.95}Si_{0.05}O_4$, cubic structure) and iron-titanium oxide JCPDS-00-054-1267 (Fe_9TiO_{15}, rhombohedral structure), where the first species

present high crystallinity, indicating a homogeneous grain growth (figure 1 item a); however, the last two compounds as such have not been reported, but in general, the elemental composition is considered characteristic of titaniferous or black sands [3, 7, 11, 12]. Likewise, in the micrograph of figure 3, section a, a regular and compact surface characteristic of magnetite can be observed, particles of clear contrast adhering to the surface are also distinguished, attributed to compounds that contain elements of lesser atomic weight. On the other hand, in sections b, and c, of the same figure 3, no particles with heavy elements immersed in the magnetite matrix were detected. Regarding the analysis by means of ICP-OES and EAAF of the MCab, it was not possible to detect the presence of gold and silver, but the content of titanium and vanadium was quantified with greater precision, being 1.17 and 0.35%, w/w, respectively. The difference in these values is due to the fact that the XRF technique is considered semi-quantitative; in addition to the above, when this technique is used in dust samples, the X-rays emitted by the elements must interact with the various crystalline structures that make up the mineral, so ISO 9516-1 is better, which indicates the fusion of borates to generate a vitreous disc [13].

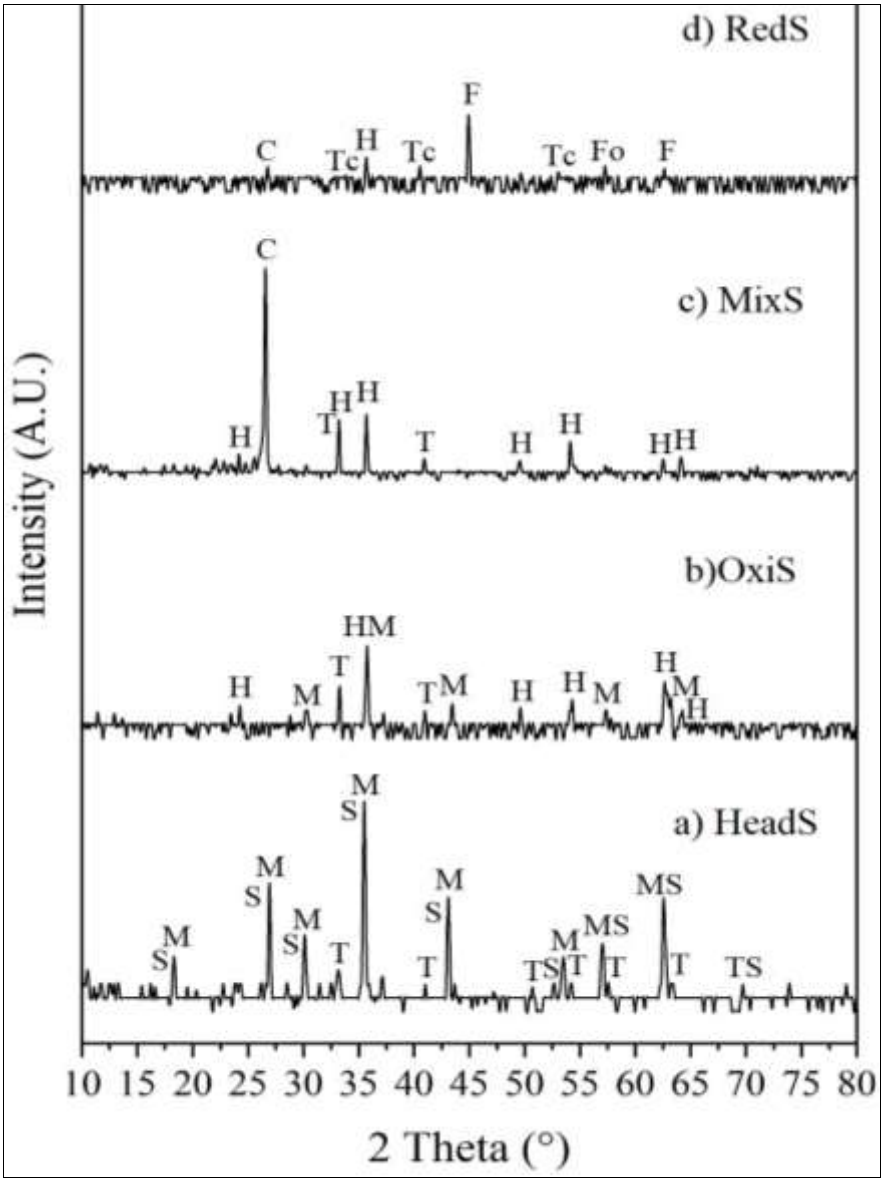

Fig 1: Diffractograms from the Head Ore, Oxidized Ore, Oxidized Ore Mixed with graphite, and Reduced Ore. Symbology: M–magnetite, S–iron-silicon oxide, T–iron-titanium oxide, H–hematite, C–graphite, F–elemental iron, Tc–titanium carbide, Fo–ferrous oxide.

Regarding oxidation, the thermogram of figure 2 shows the temperature at which the titaniferous sand begins to oxidize, initially having a slight negative slope attributed to the loss of chemisorbed moisture, continuing later with a very marked weight loss between points a, and b, due to the dihydroxylation reactions of non-metallic minerals; on the other hand, at point c there is the transformation of magnetite to hematite, at 740 °C, in accordance with what is established by the phase diagram of the Fe-O system [14]. At 800 °C (point ***d***), going down to the conversion line we have point ***d'***, which when interpolated, results in almost 20% transformation; This same procedure was repeated for the pairs ***e*** - ***e'*** and ***f*** - ***f'***, which correspond to the conversion percentages at 900 and 950 °C, being close to 40 and 50%, respectively; from the above, to achieve a higher percentage of conversion at 950 °C, long residence times and a constant supply of air to the interior of the muffle were necessary.

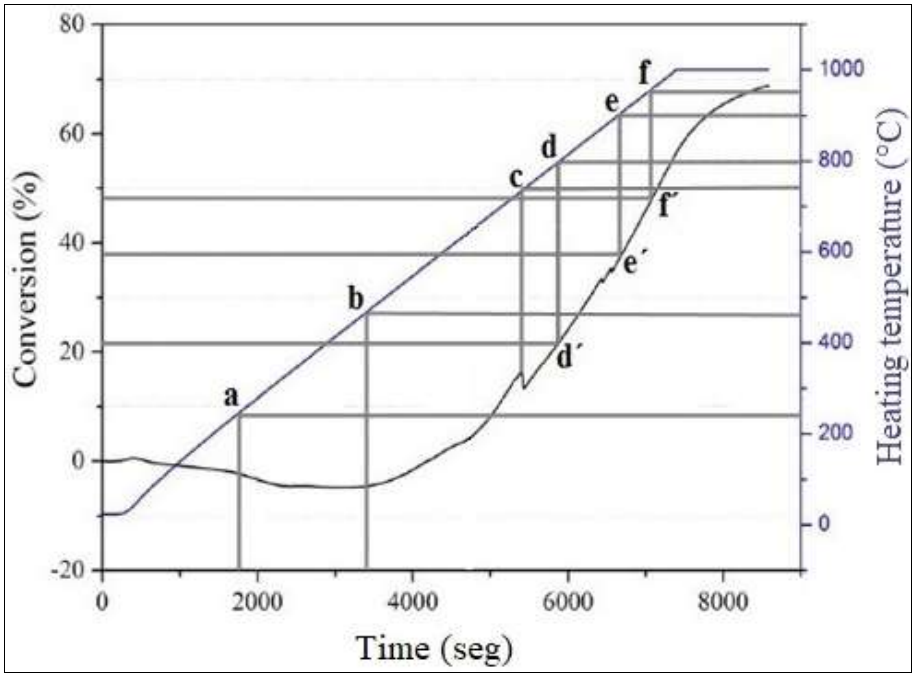

Fig 2: Thermogram resulting from the oxidation of the Head Mineral.

Oxidation Process

The hematite specie was formed in the three residence times, so that in the diffractogram of figure 1, section b, corresponding to the MOxi sample with 24 h of permanence, the hematite specie JCPDS 01-089-8104 (α phase of Fe_2O_3, rhombohedral structure) is indexed; it should be noted that the crystallinity of this phase decreases as the oxidation time increases, since the peak height is reduced and broadened, but its proportion increases, in the 12 and 24 h treatments, suggesting that the allotropic transformation of γ-Fe_2O_3 to α-Fe_2O_3 occurs after 6 h of oxidation; the magnetite species JCPDS 01-075-0449 (Fe_3O_4, cubic structure). In the micrographs in SEI mode shown in figure 3, subsection d, e, and f, a very notorious grain growth of hematite is observed, which at the beginning of oxidation are agglomerated and the non-conductive compounds are distributed homogeneously, but as the permanence in the furnace increases, the hematite grains segregate, and separate, which increases their contact area when performing the subsequent mixture with graphite.

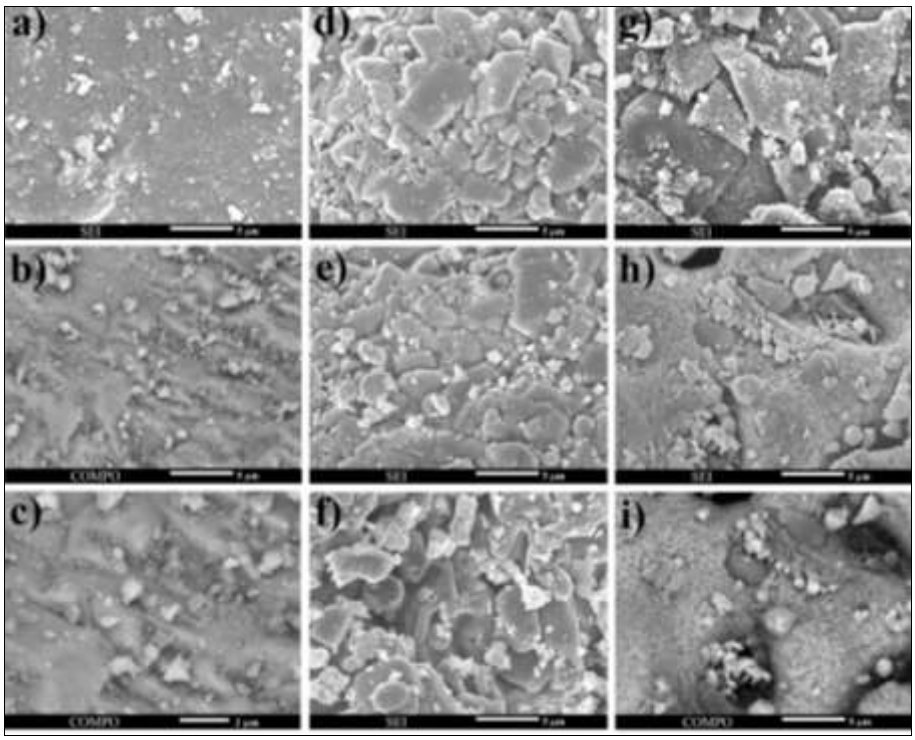

Fig 3: Secondary electron (SEI) and backscattered (COMPO) mode micrographs. a, b, c) Head Ore; d, e, f) Oxidized mineral at 6, 12 and 24 h of permanence, respectively; g) Oxidized mineral Mixed with graphite; h, i) Reduced Mineral.

Carbothermal reduction process: In the diffractogram of the MMez sample shown in figure 2, section c, the high graphite content (1:4 ratio), which was fully indexed with the JCPDS 00-026-1077 card (C, hexagonal structure), the

species of hematite (JCPDS 01-071-5088 Fe_2O_3) and iron-titanium oxide (JCPDS 01-070- 5770 $Fe_{1.696}Ti_{0.228}O_3$), both with rhombohedral structure; It is also possible to observe in the micrograph of Figure 3 (section g), how the morphology of the hematite particles is altered when mechanically mixed with the graphite, for this reason the crystallinity of these phases clearly decreases, even the residual magnetite phase cannot be indexed.

After 4 h of permanence, it is observed that the graphite phase is almost completely consumed, since in the diffractogram of the MRed sample in figure 1, item d, it is shown how the hematite was reduced to elemental iron, presenting a tall and thin peak indicative of high crystallinity (JCPDS 00-006-0696 Fe, cubic structure), the ferrous oxide species (JCPDS 00-006-0711 FeO, rhombohedral structure) is also formed by the partial reduction of hematite; Finally, there is the formation of slightly crystalline khamrabaevite due to the small and broad peak (JCPDS 00-074-1219 TiC, cubic structure), which is the product of the reduction of iron-titanium oxide. Regarding the SEM analysis, in the micrograph of figure 3 (section h), the isometric morphology of α iron is clearly observed, presenting crystals in a nodular shape and in large masses with a unit cell bcc [15], It also shows the formation of a spherical particle embedded in the iron matrix due to the slow cooling suffered by the mineral; likewise, in the micrograph in COMPO mode (figure 3, item i) the difference in phase composition is clearly observed due to the dark gray contrast of the sphere, and with the compositional chemical mapping shown in figure 4, the segregation of titanium into three particles that cannot be distinguished in COMPO mode is highlighted, it is also verified that the sphere is an oxide of silicon, since iron is absent in that area and oxygen is distributed uniformly.

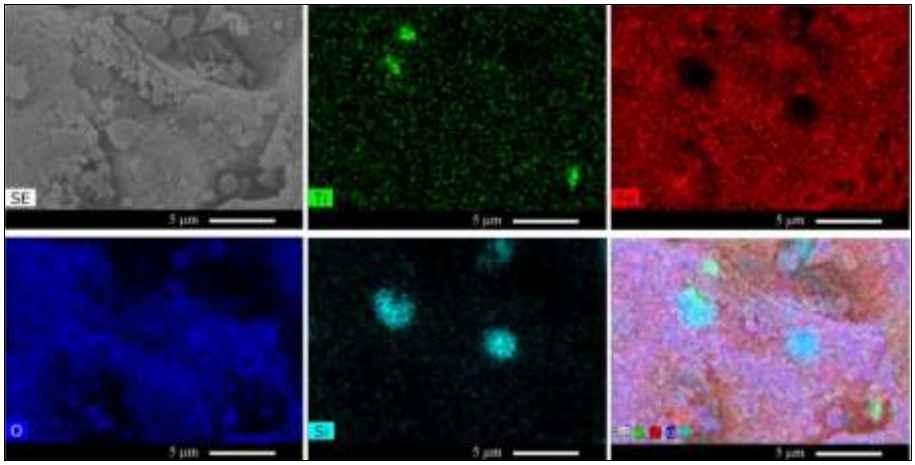

Fig 4: Chemical mapping of the Reduced Mineral with the base micrograph and the elemental patterns of titanium, iron, oxygen, and silicon.

Acid leaching of reduced ore

Figure 5, section a, shows the physical appearance of the pregnant solutions after acid leaching, observing in the MRed sample the iron dissolution effect due to the characteristic yellow coloration that this element has when it coordinates with chloride ions, while in the MCab sample, it presented a darker yellow, due to the dissolution of other elements. For its part, the MOxi sample did not present any coloration, despite the fact that in the micrograph of figure 3, section i, there is a de-agglomeration of the hematite grains, which could favor their subsequent dissolution; however, this does not occur because the solubility of hematite in hydrochloric acid is very slow [16]. Finally, the effect of the carbothermal reduction on the dissolution of vanadium, and titanium is presented in the graph of figure 5, section b, observing that in the complete digestion there was 0.34% by weight of vanadium, and 1.17% by weight of titanium, being able to dissolve 100% of the vanadium in the open leaching, and only 76.92% of the titanium present in the black beach sand, the above may be due to the formation of khamrabaevite (titanium carbide) which affects its solubility.

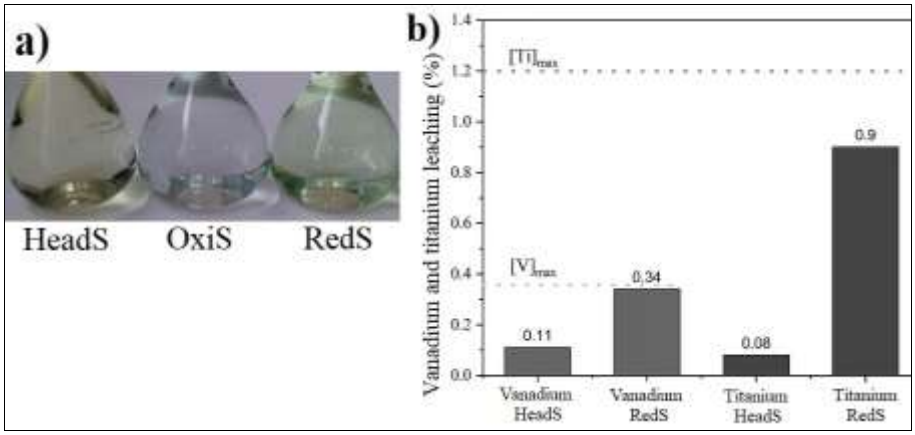

Fig 5: a) Physical appearance of the pregnant solutions after acid leaching; b) Percentage of dissolution of titanium, and vanadium before, and after carbothermal reduction.

Conclusions

From the oxidation, carbothermal reduction, and acid leaching of a mineral from the beach sand of the Pacific coast of Mexico, the following conclusions are derived:

The total dissolution of vanadium was achieved, and more than 75% of the titanium present in the titaniferous beach sand after subjecting it to a carbothermal reduction process with prior oxidation. The effectiveness of the oxidation process of the initial magnetite was verified, when transforming it into hematite, since with this the morphology of the particle was modified, going from its compact shape to unagglomerated or porous grains, increasing the contact area with the graphite, and favoring the almost complete reduction of iron as shown in the corresponding diffractogram; however, due to the molar ratio used in this work, the formation of the titanium carbide (khamrabaevite) phase, and a small amount of ferrous oxide were slightly promoted, so it is recommended to vary the ratio graphite: mineral sample, or graphite: hematite content, in future research.

Acknowledgments

The financial supports for this work from the Consejo Nacional de Ciencia y Tecnología (CONACyT) of Mexico. Hugo Jhonathan Marín-García deeply thanks to CONACyT for the scholarship during his PhD studies through the grant (444401).

Conflict of interest

The authors declare that there is no conflict of interest.

References

1. Pardave Livia W. Reciclado industrial de metales: Una aproximación. 1era ed. Ecoe. Bogotá, Col. 2006;4:87-88.
2. Chang R, College W. Química. 7ma ed. McGraw-Hill. Colombia. 2005;848:878-882.
3. Vassallo LF. Yacimientos minerales metálicos [en línea]. Universidad Nacional Autónoma de México; c2008. Querétaro. Disponible en: <http://www.geociencias.unam.mx /~bole/eboletin/lVassallo0908.pdf> [17-Feb-2023].
4. Jiménez A. Vanadio [en línea]. Disponible en: <http://www.uam.es/docencia/elementos /spV21/conmarcos/ elementos/v.html> [03-Dic-2022]
5. Vista general de la actividad minera y sus impactos [en línea]. Disponible en: <http://www.elaw.org/files/ mining-eia-guidebook/Capitulo%201.pdf> [17-Feb-2023]
6. Cortés Ruíz Velasco JF, Guillén Méndez AN. Procesos de extracción y concentración de minerales [en línea]. Universidad Nacional Autónoma de México. México DF; c2012. Disponible en: <http://galeon.com/quimica3cch/MINEROMET/Sepycon.pdf> [12-Ene-2023].
7. Vargas JA, Castañeda EA, Forero AH, Díaz SC. Obtención de hierro a partir de arenas negras del Atlántico Colombiano desembocadura Río Magdalena. [en línea], Disponible en: <http://www.invervaloresgroup.com/upload/T1-06_forero-ah_n1.pdf> [12-Ene-2023].
8. Vignes A. Extractive Metallurgy 2: Metallurgical Reaction Processes. Ed. John Wiley & Sons; c2013.
9. Yang J, Mori T, Kuwabara M. Mechanism of Carbothermic Reduction of Hematite in Hematite-Carbon Composite Pellets. Iron and Steel Institute of Japan. 2007;47(10):1394-1400.
10. Welham NJ, Williams JS. Carbothermic reduction of llmenite (FeTiO3) and rutile (TiO2). Metallurgical and Materials Transactions B. 1999;30(6):1075-1081.
11. Valderrama L, Poblete R, Contreras C. Caracterización y concentración de muestras de arenas de Caldera, Región de Atacama. Revista de la Facultad de Ingeniería, 2005, 19(38-44).
12. Alonso RN. Diccionario minero: Glosario de voces utilizadas por los mineros de Iberoamérica. 1era ed. CSIC. Madrid; c1995. p. 24.
13. Bouchard M, Milliard A, Rivard S, Ness S. ISO 9516-1 simplified borate fusion/WDXRF analytical method for iron ore including total iron analysis: Part 2. Powder Diffraction. 2014;29(2):0885-7156.
14. Birks N, Meier Gerald H, Pettit Frederick S. Introduction to the High-Temperature Oxidation of Metals. 2da ed. Cambridge University Press. United Kingdom; 2006. p. 83-85.
15. Klein C, Hurlbut CS., Manual de mineralogía. ed. Reverté; c1997. p. 377-378, 421-414, 419-422, 426-429.
16. Geolitho Stiftung gemeinnützige GmbH and other authors. Mineralienatlas – Fossilienatlas [en línea]. Disponible en: <https://www.mineralienatlas.de/lexikon/index.php/MineralData?lang=en&language= english&mineral=Hematite> [19-Abr-2023]